Slantwise Convection on Fluid Planets

Morgan E O'Neill[1] and Yohai Kaspi[1]

Key Points.

- Slantwise convection may be important in the relatively shallow weather-layer of giant planets
- At low latitudes, buoyancy perturbations yield net motion that is more horizontal than vertical
- NASA's Juno microwave measurements of Jupiter should be interpreted along angular momentum surfaces

Slantwise convection should be ubiquitous in the atmospheres of rapidly rotating fluid planets. We argue that convectively-adjusted lapse rates should be interpreted along constant angular momentum surfaces instead of lines parallel to the local gravity vector. Using Cassini wind observations of Jupiter and different lapse rates to construct toy atmospheres, we explore parcel paths in symmetrically stable and unstable weather-layers by the numerically modeled insertion of negatively buoyant bubbles. Low-Richardson number atmospheres are very susceptible to transient symmetric instability upon local diabatic forcing, even outside of the tropics. We explore parcel paths in symmetrically stable and unstable weather-layer environments, the latter by adding thermal bubbles to the weather-layer. Parcels that cool in Jupiter's belt regions have particularly horizontal paths, with implications for jetward angular momentum fluxes. These considerations may be relevant to the interpretation of Juno's ongoing observations of Jupiter's weather-layer.

1. Introduction

The fluid planets Jupiter, Saturn, Uranus and Neptune are rapidly rotating and have extensive atmospheres. The field of planetary atmospheric dynamics has generally split the work of understanding and modeling these atmospheres into two groups (see reviews by *Vasavada and Showman* [2005] and *Gerkema et al.* [2008]): the deep, well-mixed and adiabatic interiors, and the shallow, stably stratified outer weather-layers. Leading the first group, *Busse* [1976] proposed that deep atmospheric motions occur in columns and cylinders parallel with the spin axis. A large body of theory and numerical modeling work (e.g., *Christensen* [2002], *Heimpel and Aurnou* [2007], *Kaspi et al.* [2009]) demonstrates that the spin axis is the preferred direction for convective mixing for a dry adiabatic interior, for Jovian rotation rates.

[1]Department of Earth and Planetary Sciences, Weizmann Institute of Science, Rehovot, Israel.

0094-8276/16/$5.00

The second group, focusing on the thin weather layers, emphasizes the impact of stratification but uses the 'traditional approximation' of the Coriolis force [*Phillips*, 1966], wherein only the component normal to the local surface is retained: $f \approx f_0 \sin\phi$ for latitude ϕ (e.g., *Williams* [1978]; *Dowling* [1993]; *Lian and Showman* [2008]; *Liu and Schneider* [2010]). The great conceptual advantage of this is that these models can be readily modified from the more advanced Earth climate models, which typically use the traditional approximation. However, the lower boundary of these models should be much deeper than that on Earth, given previous observational evidence of the stable weather-layer depth (e.g., *Seiff et al.* [1998],*Allison and Atkinson* [2001]).

NASA's Juno spacecraft is now in Jupiter's orbit, carrying among its instruments a microwave radiometer [*Janssen et al.*, 2005] to gather passive soundings of the weather-layer and below. In light of this unprecedented data set, these two prevailing, distinct sets of assumptions and geometries appear inadequate for data interpretation, particularly in the equatorial region. The microwave observations, which are expected to retrieve trace element abundances and temperature deeper than 30 bars and into the adiabatic region, will exactly span the common limit of the shallow and deep models. Very little work has examined the impact of columnar convection in the presence of a stable stratification that is generally parallel to geopotential surfaces. One recent exception is *Heimpel et al.* [2016], who used a deep model bounded by a parameterized stable weather-layer to induce coherent surface vortices. Additional theoretical and modeling work is in order for a timely interpretation of the Juno observations.

Here we take a simple approach to explore the impact of equatorial columnar geometry on parcel motion in the weather-layer, as a function of latitude, wind shear and static stability. In Sections 2 and 3 we review symmetric instability and resulting slantwise convection, and their relation to the Richardson number. We then develop a toy steady-state model of Jupiter's outer atmosphere in Section 4, using thermal wind balance to relate Cassini-observed zonal winds to a prescribed static stability profile. This provides the basic state for the parcel model developed in Section 5. Sections 6-7 provide results, and Section 8 concludes with a discussion of assumptions and implications for the Galileo and Juno missions.

2. Symmetric instability on Earth

A parcel in a gravitationally and inertially stable atmosphere, if perturbed slightly from its origin, will oscillate about the origin. The restoring forces are buoyancy and Coriolis, respectively. Symmetric instability (SI) [*Solberg*, 1936] is a generalized framework for inertial and gravitational stabilities (see *Schultz and Schumacher* [1999], their Table 1); however, SI even in the presence of both inertial and gravitational stability is possible [*Ooyama*, 1966]. The name 'symmetric' is due to the phenomenon's two-dimensional nature. Much of SI's early terrestrially-focused development was spurred by the desire to understand mesoscale rainbands stretching latitudinally in the neighborhood of midlatitude cyclones [*Bennetts and Hoskins*, 1979; *Emanuel*, 1979, 1983a, b; *Sanders*, 1986].

SI can be diagnosed by the sign of potential vorticity (PV) [*Hoskins*, 1974]. In the Northern Hemisphere, quasi-geostrophic PV is positive everywhere, because of the assumption $f >> \zeta$, where $f = 2\Omega \sin\phi$ is the Coriolis frequency at latitude ϕ and $\zeta = \hat{k} \cdot \nabla \times \vec{u}$ is the local vertical relative vorticity (for horizontal wind $\vec{u}$). However, at the length and time scales of mesoscale systems and subsequent SI, for which the Rossby number is O(1), quasi-geostrophy no longer holds, and PV can be transiently negative. Causes include friction, diabatic heating or cooling, and cross-equatorial flow [*Dunkerton*, 1981]. More generally, SI is present wherever $f \cdot \mathrm{PV} < 0$ [*Hoskins*, 1974; *Stevens*, 1983].

Geometrically, this can be thought of as a condition on the relative orientation of angular momentum contours and potential temperature contours in a dry atmosphere. In a typical stable midlatitude atmosphere, gravitational stability requires that potential temperature (θ) increase with height. Inertial stability requires that absolute angular momentum (M) increase toward the equator. This setup is one in which the M gradient is pointed clockwise of the gradient of θ (Orientation A in Fig. 1). Colloquially, if the M surfaces are 'steeper' than the potential temperature surfaces then the atmosphere is stable to symmetric perturbations. If the potential temperature surfaces become steeper than angular momentum surfaces, such that the angular momentum gradient is now counterclockwise of the potential temperature gradient (facing Eastward in the Northern Hemisphere), the fluid is symmetrically unstable. These two perspectives on the presence of SI are equivalent because PV can be expressed as the cross product between the θ gradient and the M gradient: $\mathrm{PV} \propto \nabla\theta \times \nabla M$ [*Charney*, 1973].

3. Symmetric instability on fluid planets

Rapidly rotating fluid planets provide a model laboratory for slantwise convection studies. In slantwise convection, unstable air parcels adjust to buoyancy perturbations along absolute angular momentum surfaces instead of through purely vertical motions. Absolute angular momentum is generally oriented approximately parallel to the axis of rotation because it is dominated by the planetary rotation term, and surfaces of constant entropy are approximately parallel to geopotential surfaces. In these deep atmospheres, we can employ a more appropriate deep-shell PV, in which the Coriolis force does not vanish at the equator. However PV still vanishes at the equator because the M and θ gradients become exactly parallel [*Stevens*, 1983; *Allison et al.*, 1994]. *Gierasch and Stone* [1968] proposed that SI may be responsible for Jupiter's equatorial superrotation, though *Stone* [1971] later showed that the growth rates near the equator are very low, which we also find in the parcel motions in Section 6.

The Richardson number Ri provides a convenient measure of the likelihood that SI is present and important. It is a ratio of stratification and vertical shear,

$$Ri = \frac{N^2}{(\partial u/\partial r)^2}, \tag{1}$$

for the Brunt-Vaisala frequency $N^2 = (g/\theta_0)(\partial\theta/\partial r)$, horizontal velocity u, and depth r in spherical coordinates. *Stone* [1966] found that Ri determines the type of instability with the largest growth rate, using a hydrostatic f-plane. He found that $Ri > 0.95$ leads to growth rates that favor baroclinic instability, but that SI has the fastest growth rates in fluids with $0.25 < Ri < 0.95$. Later work by *Flasar and Gierasch* [1978] and *Hathaway et al.* [1979] did a linear stability analysis with the complete Coriolis force. The latter found a latitudinal dependence of SI on Ri due to equatorial solar insolation. *Jeffery and Wingate* [2009] determined that the range of Ri that allows SI to dominate baroclinic instabilities extends to $Ri = 2$ after considering the horizontal Coriolis component.

The study of Ri in giant planet atmospheres is still largely theoretical because there only exists one sounding of any giant planet to date: NASA's Galileo probe. *Flasar and Gierasch* [1986] and *Allison et al.* [1995] independently estimated that the Jovian Ri should be O(1) even though the Rossby number is much less than one, which in the Solar System appears unique to giant planet atmospheres (though it can also occur locally on Earth, for example in the Labrador Sea: see *Jeffery and Wingate* [2009]). This special Jovian regime is characterized by a near equivalence in vertical and horizontal temperature gradients, particularly in the equatorial region (*Allison et al.* [1995], their Fig. 3). Low Ri indicates low-PV regions throughout the weather-layer because highly tilted isentropes are more aligned with M surfaces, which provides an opportunity for SI to be induced by deep convection. Several related studies in physical oceanography examined the problem by using tilted f-planes that include a constant vertical Coriolis component [*Sun*, 1994; *Straneo et al.*, 2002; *Itano and Maruyama*, 2009; *Jeffery and Wingate*, 2009] or β-planes [*Fruman and Shepherd*, 2008]. Research into deep flows in stars also includes the full Coriolis force, though it suggests that the balanced interior flow structure is perhaps more conical than cylindrical (e.g., *Schou et al.* [1998]; *Brun et al.* [2010]).

4. A Jovian steady state atmosphere

In order to investigate the slantwise motion of perturbed parcels in Jupiter's weather-layer, we construct a toy Jovian atmosphere model that uses the Cassini-observed latitudinal profile of surface winds [*Porco et al.*, 2003] as the steady-state zonal winds at 1-bar. The wind profile is assumed to be axially symmetric and aligned along cylinders parallel to the spin axis. Initially barotropic, zonal wind u_{cyl} is made to decay inward with an e-folding depth H along the spherical-radial coordinate r, toward the center of the planet, as in *Kaspi et al.* [2010]; *Kaspi* [2013] $u(r,\phi) = u_{cyl}\exp((r-a)/H)$ for latitude ϕ and radius from planet center to 1-bar level a. This very simple base state not only excludes longitudinal variations, but also precludes meridional overturning circulations that may be concurrent with the observed belts and zones. Fig. 1 (left side) shows an example of how the winds may decay with depth. Because the depth of the winds is unknown, we allow for a range of H values. This decay depth may be constrained in the near future by the Juno gravity experiment [*Hubbard*, 1999; *Kaspi et al.*, 2010]. The winds are smoothed twice by a 0.5 degree running mean to prevent a noisy derivative necessary for thermal wind balance.

A stable lapse rate is imposed to create an outer weather-layer that mimics the stabilizing effects of solar insolation (though latitude-dependent effects are neglected), opacity and moist convection. This temperature field is modified and balanced by geostrophic thermal wind shear (e.g., *Kaspi et al.* [2009]):

$$2\Omega \frac{\partial u}{\partial Z} = -\frac{g}{\theta_0 r}\frac{\partial \theta}{\partial \phi}, \tag{2}$$

where $\partial/\partial Z = \sin\phi\partial/\partial r + \cos\phi/r\partial/\partial\phi$ for a cylindrical Z (introduced in next section).

The different lapse rate–H combinations can be characterized by the nondimensional bulk Richardson number

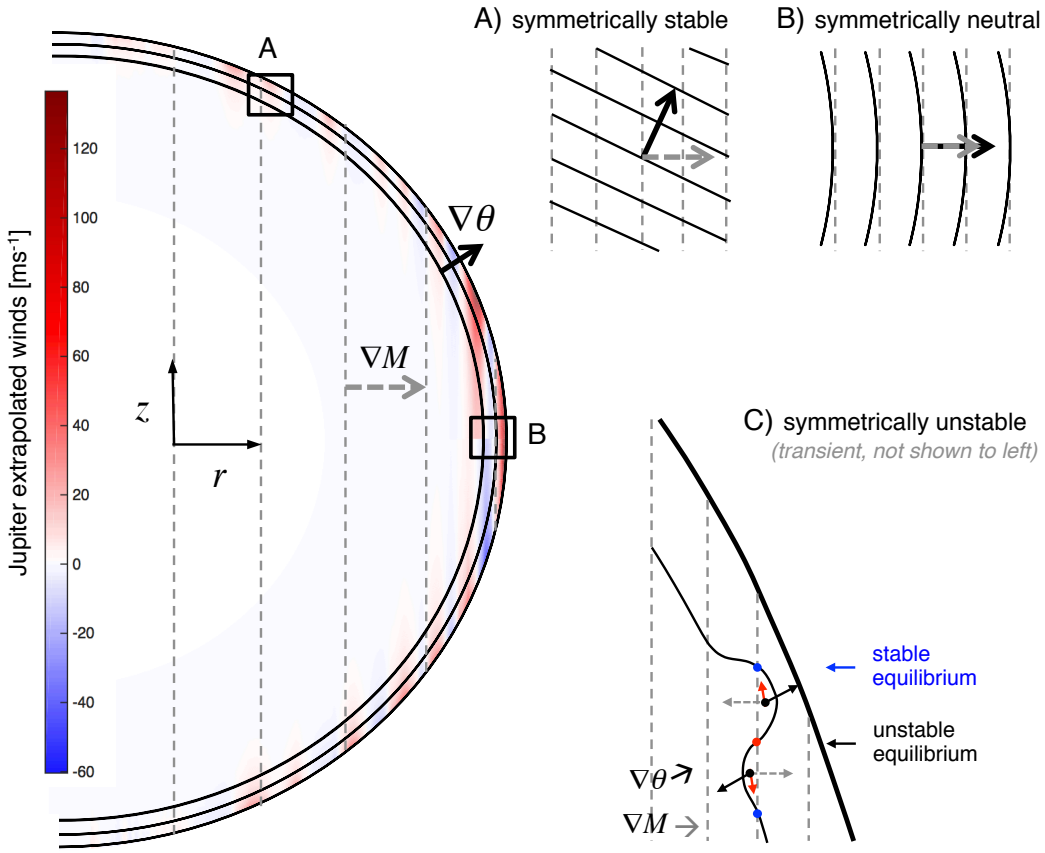

Figure 1. Left side: A not-to-scale diagram showing Cassini-observed jets (red = prograde winds, blue = retrograde winds) decaying with an e-folding scale H of 3500 km (this is unrealistically high but more easily visualized). M contours (grey dashes) and θ contours (black lines) are shown. On the right side, regions A and B are shown zoomed-in to illustrate symmetric stability and neutrality, respectively. Region C depicts a case in which transient warming at low latitudes leads to SI. A parcel originating from the red dot, upon a small perturbation, will leave its origin and oscillate about one of the two stable equilibrium positions (blue dots) due to imbalanced forces represented by thin arrows. The origin and the two stable equilibria share identical temperature and angular momentum values.

$Ri = N^2H^2/(100\text{ms}^{-1})^2$. The weather-layer lower boundary is not required to coincide with the jet terminus (departing from *Allison et al.* [1995] and *Allison* [2000]). Instead, the imposed vertical stratification is fixed to transition to an adiabatic fluid at 12 bars, with a transition thickness of $\Delta r = 15$ km and a reference potential temperature $\theta_0 = 165$ K:

$$\theta(r) = 165\text{K} - 0.5\tanh((r_{12\text{bars}} - r)/\Delta r)\frac{\partial\theta}{\partial r}dr. \quad (3)$$

In the context of SI and slantwise convection, the precise depth of the stable layer is not important. The location of the stable-to-neutral transition does not affect the relative orientation of the M and θ contours. We also examined stable layers that reached 20 bars and 50 bars to confirm that, above the transition region, there is no difference in local PV. Of more interest is the possibility that the H scale can be slightly shallower or much deeper than the weather-layer boundary.

Two extreme cases of Jupiter's Northern Hemisphere are shown on the left side of Fig. 2. On the far left is an $Ri = 840$ atmosphere. Its large H (1000 km) means wind shear is small, so thermal wind balance barely perturbs the isentropes. At the same time, static stability is high: 0.06 Kkm^{-1} .The static stability value of 0.06 Kkm^{-1} was retrieved in the upper troposphere by the Galileo probe [*Seiff et al.*, 1998] (a surprisingly high stability of 0.05 Kkm^{-1} was observed by the probe near 21 bars, and we do not consider it globally in this work). Therefore, away from the equator, the atmosphere cannot easily become symmetrically unstable due to adiabatic warming or cooling.

To the right of the $Ri = 840$ case in Fig. 2 is an $Ri = 0.7$ atmosphere, with $H = 100$ km and a stability of 0.005 Kkm^{-1}. Near the equator, the stratification appears similar to that of the high-Ri atmosphere – until 21°N is reached. Here lies Jupiter's strongest prograde jet. Because H is so low, the wind shear is very large. It visibly impacts the angular momentum distribution (grey dashes) at lower pressures. Thermal wind balance requires a proportionally large latitudinal temperature (black lines) drop across the jet. Northward, the atmosphere is barely stratified. In fact, there is a small region around 26°N that exhibits PV=0 at depth. This region is essentially neutral to buoyancy perturbations. At higher latitudes in this low-Ri case, the

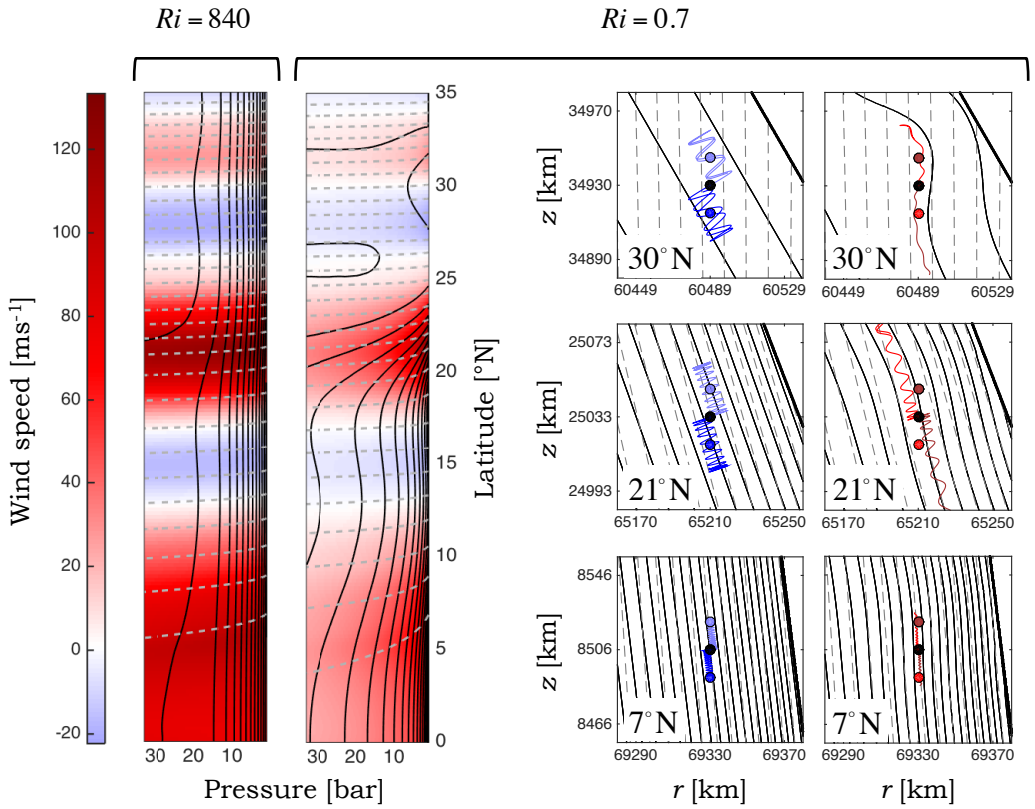

Figure 2. Left side: Northern hemisphere winds (colors), M (grey dashes) and θ (black lines) for $Ri = 840$ (far left) and $Ri = 0.7$ atmospheres. Right side: Parcel paths for the $Ri = 0.7$ case. A parcel has been moved from its origin (colored dot) to the black dot. Different colors represent independent integrations. Blue paths occur in a symmetrically stable environment. Red paths occur in a symmetrically unstable atmosphere, due to a thermal bubble superimposed upon the background stratification. To induce SI, a thermal bubble has been added to the Ri =0.7 case in the far right column. The origin is now an unstable equilibrium, so the parcel continues to move away and seek a stable equilibrium with the same temperature and angular momentum. The displacements are $dZ = \pm 15$ km. The aspect ratio of each parcel plot is 1:1; angles are true.

atmosphere even exhibits several regions of gravitational instability, which of course could never occur in a real steady state atmosphere.

The presentation of the atmosphere in the two left-most subplots in Fig. 2, while common, is rather misleading because the aspect ratio is so far from 1:1. The dashed grey M contours are still correctly parallel with the axis of rotation, the only deviations being due to strong wind shear. If these plots were narrowed to represent how comparatively small the x-axis is, the M contours would be virtually vertical at low latitudes. The subplots on the right in Fig. 2, which will be explained in Section 6, maintain the correct aspect ratio. These two atmospheres represent the extreme limits of plausible Richardson numbers. Intermediate Ri values have less extreme horizontal θ variations than the Ri=0.7 case, yet more variation than those seen in the Ri=840 case, which has an unrealistically flat meridional temperature profile.

5. A parcel model for symmetric instability

Given the background state model described above, we disturb a parcel of air (which, given imposed axial symmetry, is a zonal tube of air) and follow its subsequent path in a rotating, stratified fluid in geostrophic and hydrostatic balance. The system is expressed in cylindrical coordinates (R, Z) for distance from (and perpendicular to) the spin axis R; and distance from the equatorial plane Z, parallel to the rotation axis. This allows the full Coriolis force to be a function of one direction, R.

The equations are formulated as those in *Straneo et al.* [2002], except our coordinate system uses the spin axis as a coordinate, as opposed to the local geopotential gradient. Accordingly, we express gravity $g = 24.79\text{m s}^{-2}$ with a component $g_Z = g \sin\phi$ in the cylindrical Z direction and component $g_R = g \cos\phi$ in the R direction, for latitude ϕ from the equator. The axially symmetric, inviscid, anelastic system is:

$$\frac{\partial v}{\partial t} + \left(v\frac{\partial}{\partial R} + w\frac{\partial}{\partial Z} \right) v - 2\Omega u = -\frac{1}{\rho_0}\frac{\partial p}{\partial R} - g_R \frac{\theta}{\theta_0} \quad (4)$$

$$\frac{\partial u}{\partial t} + \left(v\frac{\partial}{\partial R} + w\frac{\partial}{\partial Z} \right) u + 2\Omega v = 0 \quad (5)$$

$$\frac{\partial w}{\partial t} + \left(v\frac{\partial}{\partial R} + w\frac{\partial}{\partial Z} \right) w = -\frac{1}{\rho_0}\frac{\partial p}{\partial Z} - g_Z \frac{\theta}{\theta_0} \quad (6)$$

$$\frac{D\theta}{Dt} = 0 \quad (7)$$

The material derivative is $D/Dt = v\partial/\partial R + w\partial/\partial Z$, θ_0= 165 K is a reference dry potential temperature, and

$\rho_0 = \rho_0(z)$ is a function of local depth. The leading order balances for small Rossby number are:

$$-2\Omega\bar{u} = -\frac{1}{\rho_0}\frac{\partial\bar{p}}{\partial R} - g_R\frac{\bar{\theta}}{\theta_0}, \quad (8)$$

$$0 = -\frac{1}{\rho_0}\frac{\partial\bar{p}}{\partial Z} - g_Z\frac{\bar{\theta}}{\theta_0} \quad (9)$$

where axisymmetric steady states are indicated by an overbar. The $g_R\bar{\theta}/\theta_0$ term is maximum at the equator and zero at the pole; the inverse is true for $g_Z\bar{\theta}/\theta_0$. Cross-differentiation of these balances yields the thermal wind relation (Eq. 2). At high latitudes, Eqs. 2-2 are similar to geostrophic and hydrostatic balance, respectively.

We consider the equations of motion for a parcel displaced from its orginal location. Let $M = u + 2\Omega R$ be the conserved absolute angular momentum of the fluid [*Eliassen*, 1962; *Emanuel*, 1983a, b] appropriate for axially symmetric geostrophic balance. Here M is actually a pseudo-angular momentum as in *Emanuel* [1983b], but we will refer to it throughout as angular momentum.

The parcel method of determining stability does not linearize motions, but it does neglect the pressure perturbation forces experienced by the parcel. Turbulent mixing, which would break axial symmetry of the following motions, is also neglected and this will limit the distance over which the following equations are valid. However, *Stevens* [1983] showed that in the inviscid case the neglected associated forces have smaller magnitudes than the retained Coriolis force. Modified from *Emanuel* [1983a, b]; *Straneo et al.* [2002], the equations of motion away from the balanced state are:

$$\frac{DM}{Dt} = 0, \quad (10)$$

$$\frac{Dv}{Dt} = f(M - \bar{M}) + \frac{g_R}{\theta_0}(\theta - \bar{\theta}), \quad (11)$$

$$\frac{Dw}{Dt} = \frac{g_Z}{\theta_0}(\theta - \bar{\theta}). \quad (12)$$

The basic states $\bar{M}$ and $\bar{\theta}$ are determined by the thermal wind balanced jet model discussed in Section 4. In the following path integrations, the initial conditions are for $t = t_0$, $v = w = 0$. The equations of motion are discretized with a 2nd order Adams-Bashforth time stepping scheme. Integrations are insensitive to changes in spatial and temporal resolution that adequately resolve the higher-frequency buoyancy oscillations.

6. Parcel displacements

From Eqs. 11-12 we can immediately deduce the motions following a range of displacements. For a parcel perturbed from its origin in a symmetrically stable atmosphere, the parcel will oscillate about its origin with a frequency in each dimension proportional to the relevant stratification. In a symmetrically unstable atmosphere (e.g., Fig. 1) a parcel will leave its unstable equilibrium and move to find the next stable equilibrium. For instabilities near the surface, the next stable equilibrium point may not exist (because it would lie outside the planet), and in that case the idealized parcel will reach the surface with a high velocity.

At high latitudes, where orientations of both $\bar{M}$ and $\bar{\theta}$ are similar those of the terrestrial high latitudes, g_R will be negligible, leaving the horizontal equation of motion to adjust states to inertial stability, and the vertical equation to adjust states to gravitational stability. Near the equator, the temperature and angular momentum surfaces are nearly parallel. Additionally, g_Z is virtually zero. The oscillation about the origin due to vertical displacements is accordingly so slow that such displacements can be viewed as irreversible.

Three tropical Northern hemisphere latitudes, 30°N, 21°N and 7°N, are shown for comparison of stable and unstable parcel motion in the $Ri = 0.7$ atmosphere (Fig. 2, right side). Parcels have been moved from their origin to the black dot, ±15 km away in the Z-direction, and released, and the integration shown takes place over 10 hours (≈ one Jovian day). Blue paths are due to displacement from a stable origin, and red paths indicate an unstable origin. The difference between the stratification at 21°N and 30°N is dramatic and is due to the very low Ri, which enhances the effect of thermal wind balance. The buoyancy oscillations are visibly less frequent at 30°N because the stratification is so low. We also show parcel motion at 7°N, where the Galileo probe entered Jupiter's atmosphere.

In the $Ri \approx 840$ case, the strong stratification is barely modified by thermal wind balance, and it prohibits weak diabatic warming or cooling from inducing SI except for a region very close to the equator (not shown). Even if SI were to occur regularly, Ri is so large that the growth rate of baroclinic instability would exceed that of SI [*Gierasch and Stone*, 1968].

The rightmost column of Fig. 2 is identical to the middle column except for the presence of a cold thermal bubble superimposed on the background temperature field to induce SI. The bubble represents a local disturbance due to convection or diabatic cooling to space, and is a 2D Gaussian with full-width half-maximum radius of 30 km, a depth below 1-bar of 50 km, and perturbation temperature of −0.25 K. Here we neglect to re-adjust the background winds to thermal wind balance with the thermal bubble. The impact of a full thermal wind balance to a weak thermal bubble would be small, but in fact favorable for SI on the equatorward side of the bubble (the absolute angular momentum will be tilted counterclockwise from the vertical), exactly where SI occurs and where we place and release the parcels. Similar reasoning holds for a warm bubble (not shown): SI would occur on the poleward flank, which is also where thermal wind adjustment would tend to increase it.

In the presence of the cold thermal bubble, temperature contours are now oriented *clockwise* of the angular momentum contours, rendering PV locally negative to the immediate south of the bubble center (see schematic 'C' in Fig. 1). The resulting SI forces displaced parcels away from their origin while they execute a buoyancy oscillation around the original temperature surface. These parcels will continue to move toward the next stable equilibrium location with the same temperature and angular momentum as the origin and then oscillate around that new equilibrium.

Whether in environments of symmetric stability or instability, parcels displaced at low latitudes move extremely slowly in the vertical direction because both g_Z and $\theta - \bar{\theta}$ are very small. Motions in the Z-direction that are already preferred by angular momentum conservation are now barely inhibited by stratification. At 7°N (bottom row) a displaced parcel reaches its origin within a day. At 2°N (not shown) the parcel travels only 10% of the way to the origin within a day.

This has implications for convection in the equatorial region. Even in a highly stratified troposphere, there is virtually no inhibition to (cylindrical) vertical displacements. For a real tube of air, the assumptions of symmetric stability, in particular that of along-tube uniformity, would break down before the tube would ever return to its origin. In this

sense the equatorial region is effectively unstable to vertical displacements.

The characteristic timescale for baroclinic instability is $\sqrt{Ri}/(2\Omega \sin\phi)$, while the SI timescale is $1/(2\Omega)$. Previous theoretical work [*Stone*, 1971] showed that equatorial regions should experience "slow-growing, low-latitude" SI modes, which Stone proposed could explain low-latitude cloud band observations on Jupiter. Because the timescale for baroclinic instability reaches infinity at the equator, slow SI motions can still dominate weather-layer features. In fact, SI is not even required for slantwise convection to alter the flow field because cylindrically vertical displacements are effectively irreversible.

7. A ventilated Jovian thermocline?

For the $Ri = 0.7$ atmosphere, the temperature drop across the 21°N prograde jet (from 20°N to 22°N) at 1-bar is ≈2.5 K. These isentropes intersect the emission level of Jupiter and provide a diabatic PV sink via radiation to fluid layers that would otherwise conserve PV, as in the ocean ventilated thermocline of *Luyten et al.* [1983] (we disregard moisture, though it can also affect PV significantly). The atmosphere may cool preferentially in the belts of Jupiter, which are cyclonic bands poleward of prograde jets. Likely due to a combination of low opacity and relatively cloud-free regions, they appear to be relatively warm, in contrast to the high clouds of the zones. A parcel that cools just poleward of the 21°N jet would descend downward and equatorward until it reaches and oscillates about its new, cooler equilibrium (Fig. 3). The angular momentum surfaces are also tilted by the strong prograde winds. These factors force the parcel, which lost buoyancy but not angular momentum, to move in a highly slantwise fashion. In Fig. 3, a parcel that starts at the black circle cools by either 1, 0.5 or 0.25 K, and immediately responds to the buoyancy perturbation by falling radially inward. While executing a buoyancy oscillation around the new equilibrium temperature (different in each case), each parcel seeks a new location where the new θ surface intersects the previous M surface (same in all cases). Thus the parcel moves southward horizontally - in this case at an angle merely 7° from a geopotential surface, or a full horizontal kilometer for every 120 m in depth. The tilt is increasingly horizontal at lower latitudes. The belt regions therefore provide a more effective conveyor for dense fluid parcels to move to lower latitudes than the anticyclonic zones.

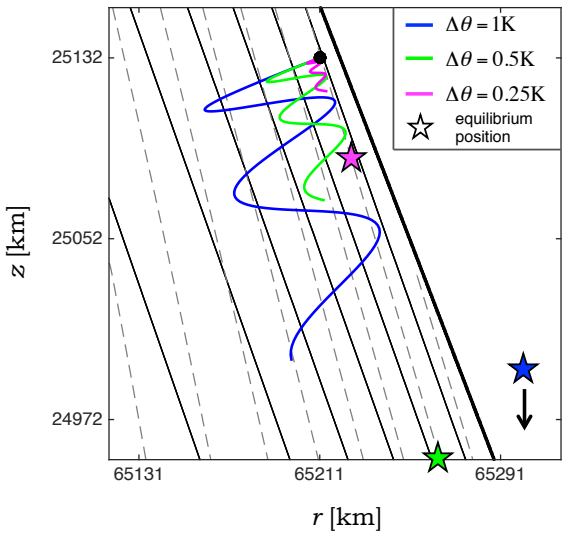

Figure 3. Parcel paths at 21°N for $d\theta/dZ = 0.005$ Kkm^{-1} and $H = 100$ km. Grey dashes are M surfaces and black lines are θ surfaces. A parcel is placed near the 1-bar boundary (it lies slightly deeper because of numerical edge effects). Each color shows the path after an instantaneous cooling of 1, 0.5 or 0.25 K. The parcels move downward and equatorward toward a cooler temperature contour that intersects with the original angular momentum, while undergoing rapid buoyancy oscillations. The stars mark the new equilibrium position of the parcel, and they must lie along the same M surface as the original parcel location, because in this example M is conserved while the parcel cools. The blue equilbrium position is beyond plot limits, though it too would lie on the original grey M surface. The integration period is 2 hours and the aspect ratio is 1:1.

SI induces parcel motion that usually follows or oscillates around surfaces of constant θ because $N^2 > (2\Omega)^2$. However, the end result is that convection mixes air on surfaces of constant M. *Emanuel* [1983a] observed that during parcel motion, due to the transient difference in parcel and background M values, there is an instantaneous M flux with a horizontal component up-gradient (while overall the flux is downgradient). In the case of preferential cooling in Jovian belts, this implies a possible M flux convergence into the jets immediately equatorward of the belts. Future numerical studies should endeavor to resolve Rossby number O(1) motions in the Jovian weather-layer to determine whether slantwise convection is an important angular momentum source or sink for the jets.

8. Discussion

This study has looked at how axial convection may behave within a Jovian weather-layer. Because motion is restricted to be purely zonal, there is no meridional overturning to motivate differing lapse rates under belts and zones, and so the lapse rate varies only due to thermal wind balance. In constructing a family of atmospheres with varying

Ri, we found that it was difficult to avoid gravitationally unstable weather-layers for low *Ri*. Furthermore, the jets are thought to extend much deeper than the O(100) km depth of the weather-layer, consistent with the Galileo probe wind measurements [*Atkinson et al.*, 1997]. Below the prescribed weather-layer, the model is assumed to be adiabatic everywhere. Thermal wind at low latitudes can stretch the stratified region well beyond the prescribed 12 bar limit. At higher latitudes, thermal wind balance can overturn the fluid altogether and forces negative gravitational stability. A real fluid of course would not tolerate such a steady state - but this does suggest that the different expectations for the weather-layer depths (possibly shallow) and jet depths (possibly deep) need to be considered in concert. *Allison* [2000] avoids this problem by defining a lower boundary layer of no motion, and allowing thermal wind to balance the fluid above consistently as winds increase. Models that instead assume deep winds without accounting for the lower adiabatic boundary allow thermal wind to create strong horizontal temperature gradients, with no clear resolution at the bottom boundary (e.g., *Liu et al.* [2013]).

The impact of latent heating, apart from a partial justification for a stable troposphere, has been neglected in this study but should be very complex and influential [*Stoker*, 1986; *Li and Ingersoll*, 2015]. Also, baroclinic instability is not permitted in such a model because it would require the breaking of axial symmetry, and accordingly the long path lengths demonstrated here are very likely to be disturbed by other dynamical instabilities along the way. These effects must be accounted for before we can draw stronger conclusions about the biases that symmetric instability provides to the general circulation.

Convective motions on the giant planets challenge the traditional notions of up and down. While buoyancy acts parallel to gravitational acceleration, the angular momentum constraint on motion means that the dominance of slantwise convection is a function of latitude. The Galileo probe pierced the Jovian atmosphere at 7°N, with a trajectory close to parallel with gravity by the time it reached about 1 bar. The resulting atmospheric profile was a surprise to many: the atmosphere was remarkably stable and dry, with a lapse rate of approximately 0.06 Kkm^{-1} in the upper troposphere, increasing to as much as 0.5 Kkm^{-1} at a depth of 22 bars [*Seiff et al.*, 1998]. A forthcoming study will include a re-examination of the Galileo probe sounding in order to measure convective adjustment along angular momentum surfaces instead of the local vertical direction. Assessing only the latter can be misleading, causing adiabatic fluids to appear stably stratified [*Emanuel*, 1983a, 1985; *Straneo et al.*, 2002]. The ongoing microwave experiment aboard the Juno spacecraft will provide a rich dataset for assessing impact of slantwise convective adjustment at all latitudes.

Acknowledgments. The authors gratefully acknowledge support from the Israeli Ministry of Science, the Minerva Foundation with funding from the Federal German Ministry of Education and Research, the Weizmann Institute of Science (WIS) Helen Kimmel Center for Planetary Science, the WIS Dean's Postdoctoral Fellowship and the WIS Postdoctoral Koshland Prize. The data used in this study are listed in the references below.

References

Allison, M., A. D. Del Genio, and W. Zhou (1994), Zero potential vorticity envelopes for the zonal-mean velocity of the Venus/Titan atmospheres, *J. Atmos. Sci.*, *51*(5), 694–702.

Allison, M., A. D. Del Genio, and W. Zhou (1995), Richardson number constraints for the Jupiter and outer planet wind regime, *Geophys. Res. Lett.*, *22*(21), 2957–2960.

Allison, M., (2000), A similarity model for the windy Jovian thermocline, *Plan. and Space Sci.*, *48*(7-8), 753–774.

Allison, M., and D. Atkinson (2001), Galileo probe Doppler residuals as the wave-dynamical signature of weakly stable, downward-increasing stratification in Jupiter's deep wind layer, *Geo. Res. Lett.*, *28*(14), 2747–2750.

Atkinson, D. H., A. P. Ingersoll, and A. Seiff (1997), Deep winds on Jupiter as measured by the Galileo probe, *Nature*, *388*(6643), 649-650.

Bennetts, D. A., and B. J. Hoskins (1979), Conditional symmetric instability - a possible explanation for frontal rainbands, *Q. J. Royal Met. Soc.*, *105*(446), 945–962.

Brun, A. S., H. M. Antia, and S. M. Chitre (2010), Is the solar convection zone in strict thermal wind balance? *Astron. Astrophys*, *510*, A33.

Busse, F. H. (1976), A simple model of convection in the Jovian atmosphere, *Icarus*, *29*(2), 255–260.

Charney, J. G. (1973), *Dynamic Meteorology: Lectures Delivered at the Summer School of Space Physics of the Centre National D'Etudes Spatiales, Held at Lannion, France, 7 August–12 September 1970*, chap. Planetary Fluid Dynamics, pp. 97–351, Springer Netherlands, Dordrecht.

Christensen, U. R. (2002), Zonal flow driven by strongly supercritical convection in rotating spherical shells, *J. Fluid Mech.*, *470*, 115–133.

Dowling, T. E. (1993), A relationship between potential vorticity and zonal wind on Jupiter, *J. Atmos. Sci.*, *50*(1), 14–22.

Dunkerton, T. J. (1981), On the inertial stability of the equatorial middle atmosphere, *J. Atmos. Sci.*, *38*(11), 2354–2364.

Eliassen, A. (1962), On the vertical circulation in frontal zones, *Geofys. Publik.*, *24*, 147–160.

Emanuel, K. A. (1979), Inertial instability and mesoscale convective systems. part i: Linear theory of inertial instability in rotating viscous fluids, *J. Atmos. Sci.*, *36*(12), 2425–2449.

Emanuel, K. A. (1983a), The Lagrangian parcel dynamics of moist symmetric instability, *J. Atmos. Sci.*, *40*(10), 2368–2376.

Emanuel, K. A. (1983b), On assessing local conditional symmetric instability from atmospheric soundings, *Mon. Weather Rev.*, *111*(10), 2016–2033.

Emanuel, K. A. (1985), Convective adjustment in baroclinic atmospheres, in *The Jovian Atmospheres*, edited by M. Allison and L. D. Travis, no. 2441 in Conference Proceedings, pp. 163–171, NASA, NASA Scientific and Technical Information Branch, New York, New York.

Flasar, F. M., and P. J. Gierasch (1978), Turbulent convection within rapidly rotating superadiabatic fluids with horizontal temperature gradients, *Geophys. & Astrophys. Fluid Dyn.*, *10*(1), 175–212.

Flasar, F. M., and P. J. Gierasch (1986), Mesoscale waves as probe of Jupiter's deep atmosphere, *J. Atmos. Sci.*, *43*, 2683–2707.

Fruman, M. D., and T. G. Shepherd (2008), Symmetric stability of compressible zonal flows on a generalized equatorial -plane, *J. Atmos. Sci.*, *65*(6), 1927–1940.

Gerkema, T., J. T. F. Zimmerman, L. R. M. Maas, and H. van Haren (2008), Geophysical and astrophysical fluid dynamics beyond the traditional approximation, *Rev. of Geophysics*, *46*(2).

Gierasch, P. J., and P. H. Stone (1968), A mechanism for jupiter's equatorial acceleration, *J. Atmos. Sci.*, *25*(6), 1169–1170.

Hathaway, D. H., P. A. Gilman, and J. Toomre (1979), Convective instability when the temperature gradient and rotation vector are oblique to gravity. i. fluids without diffusion, *Geophys. & Astrophys. Fluid Dyn.*, *13*(1), 289–316.

Heimpel, M., and J. Aurnou (2007), Turbulent convection in rapidly rotating spherical shells: A model for equatorial and high latitude jets on Jupiter and Saturn, *Icarus*, *187*(2), 540–557.

Heimpel, M., T. Gastine, and J. Wicht (2016), Simulation of deep-seated zonal jets and shallow vortices in gas giant atmospheres, *Nature Geosci.*, *9*(1), 19–23.

Hoskins, B. J. (1974), The role of potential vorticity in symmetric stability and instability, *Q. J. Royal Met. Soc.*, *100*(425), 480–482.

Hubbard, W. B. (1999), Gravitational signature of Jupiter's deep zonal flows, *Icarus*, *137*(2), 357–359.

Itano, T. and K. Maruyama, Symmetric stability of zonal flow under full-component Coriolis force – Effect of the horizontal component of the planetary vorticity, *J. Meteo. Soc. Japan, Ser. II*, *87*(4), 747–753.

Janssen, M. A., M. D. Hofstadter, S. Gulkis, A. P. Ingersoll, M. Allison, S. J. Bolton, S. M. Levin, and L. W. Camp (2005), Microwave remote sensing of Jupiter's atmosphere from an orbiting spacecraft, *Icarus*, *173*(2), 447–453.

Jeffery, N., and B. Wingate (2009), The effect of tilted rotation on shear instabilities at low stratifications, *J. Phys. Ocean.*, *39*(12), 3147–3161.

Kaspi, Y., G. R. Flierl, and A. P. Showman (2009), The deep wind structure of the giant planets: Results from an anelastic general circulation model, *Icarus*, *202*(2), 525–542.

Kaspi, Y., W. B. Hubbard, A. P. Showman, and G. R. Flierl (2010), Gravitational signature of Jupiter's internal dynamics, *Geophys. Res. Lett.*, *37*(1), L01204.

Kaspi, Y. (2013), Inferring the depth of the zonal jets on Jupiter and Saturn from odd gravity harmonics, *Geophys. Res. Lett.*, *40*, 676-680.

Li, C., and A. P. Ingersoll (2015), Moist convection in hydrogen atmospheres and the frequency of Saturn[rsquor]s giant storms, *Nature Geosci.*, *8*(5), 398–403.

Lian, Y., and A. P. Showman (2008), Deep jets on gas-giant planets, *Icarus*, *194*(2), 597–615.

Liu, J., and T. Schneider (2010), Mechanisms of jet formation on the giant planets, *J. Atmos. Sci.*, *67*(11), 3652–3672.

Liu, J., T. Schneider, and Y. Kaspi (2013), Predictions of thermal and gravitational signals of Jupiter's deep zonal winds, *Icarus*, *224*(1), 114–125.

Luyten, J. R., J. Pedlosky, and H. Stommel (1983), The ventilated thermocline, *J. Phys. Oceanogr.*, *13*(2), 292–309.

Ooyama, K. (1966), On the stability of the baroclinic circular vortex: a sufficient criterion for instability, *J. Atmos. Sci.*, *23*(1), 43–53.

Phillips, N. A. (1966), The equations of motion for a shallow rotating atmosphere and the "traditional approximation", *J. Atmos. Sci.*, *23*(5), 626–628.

Porco, C. C., R. A. West, A. McEwen, A. D. Del Genio, A. P. Ingersoll, P. Thomas, S. Squyres, L. Dones, C. D. Murray, T. V. Johnson, J. A. Burns, A. Brahic, G. Neukum, J. Veverka, J. M. Barbara, T. Denk, M. Evans, J. J. Ferrier, P. Geissler, Helfenstein, T. Roatsch, H. Throop, M.Tiscareno, A. R. Vasavada (2003), Cassini Imaging of Jupiter's Atmosphere, Satellites and Rings, *Science*, *299*(5612), 1541–1547.

Sanders, F. (1986), Frontogenesis and symmetric stability in a major New England snowstorm, *Mon. Weather Rev.*, *114*, 1847–1862.

Schou, J., H. M. Antia, S. Basu, R. S. Bogart, R. I. Bush, S. M. Chitre, J. Christensen-Dalsgaard, M. P. Di Mauro, W. A. Dziembowski, A. Eff-Darwich, D. O. Gough, D. A. Haber, J. T. Hoeksema, R. Howe, S. G. Korzennik, A. G. Kosovichev, R. M. Larsen, F. P. Pijpers, P. H. Scherrer, T. Sekii, T. D. Tarbell, A. M. Title, M. J. Thompson, and J. Toomre, (1998), Helioseismic studies of differential rotation in the solar envelope by the Solar Oscillations Investigation using the Michelson Doppler Imager, *J. Astrophys. J.*, *505*, 390–417.

Schultz, D. M., and P. N. Schumacher (1999), The use and misuse of conditional symmetric instability, *Mon. Weather Rev.*, *127*(12), 2709–2732.

Seiff, A., D. B. Kirk, T. C. D. Knight, R. E. Young, J. D. Mihalov, L. A. Young, F. S. Milos, G. Schubert, R. C. Blanchard, and D. Atkinson (1998), Thermal structure of Jupiter's atmosphere near the edge of a 5-m hot spot in the north equatorial belt, *J. Geophys. Res. (Planets)*, *103*(E10), 22,857–22,889.

Solberg, H. (1936), Le mouvement d'inertie de l'atmosphère stable et son rôle dans la théorie des cyclones, *Proc. -verb. Assoc. météor. U.G.G.I. (Edinburgh)*, *pt. II (Mém.)*, 66–82.

Stevens, D. E. (1983), On symmetric stability and instability of zonal mean flows near the equator, *J. Atmos. Sci.*, *40*(4), 882–893.

Stoker, C. R. (1986), Moist convection: A mechanism for producing the vertical structure of the jovian equatorial plumes, *Icarus*, *67*(1), 106–125.

Stone, P. H. (1966), On non-geostrophic baroclinic stability, *J. Atmos. Sci.*, *23*(4), 390–400.

Stone, P. (1967), An application of baroclinic stability theory to the dynamics of the jovian atmosphere, *J. Atmos. Sci.*, *24*, 642–652.

Stone, P. (1971), The symmetric baroclinic instability of an equatorial current, *Geophys. Fluid Dyn.*, *2*(1), 147–164.

Straneo, F., M. Kawase, and S. C. Riser (2002), Idealized models of slantwise convection in a baroclinic flow, *J. Phys. Ocean.*, *32*(2), 558–572.

Sun, W.-Y. (1994), Unsymmetrical symmetric instability, *Q. J. Royal Met. Soc.*, *121*(522), 419–431.

Vasavada, A. R., and A. P. Showman (2005), Jovian atmospheric dynamics: an update after Galileo and Cassini, *Reports on Progress in Physics*, *68*(8), 1935–1993.

Williams, G. P. (1978), Planetary circulations: I. Barotropic representation of Jovian and terrestrial turbulence, *J. Atmos. Sci.*, *35*(8), 1399–1426.

Corresponding author: Morgan E O'Neill, Department of Earth and Planetary Sciences, Weizmann Institute of Science, Rehovot, Israel (morgan.e.oneill@gmail.com)